Physica B: Condensed Matter 537 (2018) 194–201

Contents lists available at ScienceDirect

Physica B: Condensed Matter

journal homepage: www.elsevier.com/locate/physb

Temperature-dependent infrared optical properties of 3C-, 4H- and 6H-SiC

Zhen Tong [a], Linhua Liu [b], Liangsheng Li [c,*], Hua Bao [a,**]

[a] University of Michigan-Shanghai Jiao Tong University Joint Institute, Shanghai Jiao Tong University, Shanghai 200240, China
[b] School of Energy Science and Engineering, Harbin Institute of Technology, Harbin 150001, China
[c] Science and Technology on Electromagnetic Scattering Laboratory, Beijing 100854, China

ARTICLE INFO

Keywords:
SiC polytypes
Infrared phonon mode
Temperature-dependent optical properties
First-principles calculations

ABSTRACT

The temperature-dependent optical properties of cubic (3C) and hexagonal (4H and 6H) silicon carbide are investigated in the infrared range of 2–16 μm both by experimental measurements and numerical simulations. The temperature in experimental measurement is up to 593 K, while the numerical method can predict the optical properties at elevated temperatures. To investigate the temperature effect, the temperature-dependent damping parameter in the Lorentz model is calculated based on anharmonic lattice dynamics method, in which the harmonic and anharmonic interatomic force constants are determined from first-principles calculations. The infrared phonon modes of silicon carbide are determined from first-principles calculations. Based on first-principles calculations, the Lorentz model is parameterized without any experimental fitting data and the temperature effect is considered. In our investigations, we find that the increasing temperature induces a small reduction of the reflectivity in the range of 10–13 μm. More importantly, it also shows that our first-principles calculations can predict the infrared optical properties at high-temperature effectively which is not easy to be obtained through experimental measurements.

1. Introduction

Silicon carbide (SiC) is a semiconductor with wide band gap and low carrier concentration, which has extensive applications in high-temperature, high-frequency, high-power and high-voltage electronic device engineering, and has also been widely used in optoelectronic devices [1–5]. More importantly, due to the excellent optical properties, SiC has the great potential application in civil, commercial, military and aerospace vehicles as a candidate of high-temperature electromagnetic wave absorbing materials [6,7]. From the physical point of view, it exhibits interesting structural properties. Due to the different stacking sequence of Si-C bilayers, it exists about 250 different polymorph crystallizing in the cubic (zinc-blend, C), hexagonal (wurtzite, H), and rhombohedral (R) lattice structure [8]. Among these polytypes, the 3C-, 4H- and 6H-SiC are the most commonly encountered polymorph.

Experimental investigations have been widely carried out to obtain the finite temperature optical properties of SiC polytypes in the past decades. For example, the infrared reflectivity of cubic SiC (3C-SiC) was measured at room temperature using different techniques including a double-pass Perkin Elmer spectrometer [9,10], Fourier Transform Infrared (FTIR) [11,12] spectrometer and spectroscopic ellipsometry [13]. Yang *et al.* [14] measured the dielectric properties in the temperature range of 373–773 K at gigahertz range (8.2–12.4 GHz). Petalas *et al.* [15] ellipsometrically measured the optical properties of 3C- and 6H-SiC in the temperature range of 90–550 K and in the energy region from 5 to 10 eV. With the aid of spectroscopic ellipsometry, Cobet *et al.* [16] experimentally measured the optical properties of 3C-, 4H- and 6H-SiC at 300 K in the energy range from 3.5 to 10 eV. However, it is not easy to directly measure the infrared optical properties at high temperature due to the limitation of self-radiation and thermal oxidation [17]. Furthermore, these temperature-dependent experimental measurements of optical properties mainly focused in the ultraviolet range, while the temperature-dependent optical properties in infrared region have not been mentioned to our knowledge.

In addition to the experimental measurements, there are extensive numerical simulation works have been widely carried out to investigate the optical properties of SiC. For instance, Bechstedt *et al.* [8] implemented the first-principles method to compute dielectric function of 3C-, 4H- and 6H-SiC in the energy range of 5–15 eV. Xie *et al.* [18] investigated the optical properties of 6H-SiC with the ab initio full potential augmented plane wave method. Lambercht *et al.* [19] studied the ultraviolet optical properties of 3C-, 2H-, 4H- and 6H-SiC based on

* Corresponding author.
** Corresponding author.
E-mail addresses: liliangshengbititp@163.com (L. Li), hua.bao@sjtu.edu.cn (H. Bao).

https://doi.org/10.1016/j.physb.2018.02.023
Received 26 December 2017; Accepted 12 February 2018
Available online 13 February 2018
0921-4526/

first-principles calculations. However, these studies only predict the optical properties of SiC at ground state and temperature effect is not considered. In order to compute the temperature effect on optical properties of SiC. Domingues *et al.* [20] implemented the molecular dynamics simulation to study the influence of temperature and pressure on the optical properties of undoped 3C-SiC structures, in which the empirical potential needed to be developed. Nevertheless, this method is much available for the diatomic ionic material with cubic symmetry (3C-SiC) and is not easily applied to the 4H- and 6H-SiC with complicated unit cell structure. Yang *et al.* [21] investigated the dielectric function of 3C- and 6H-SiC in the temperature range of 90–538 K and in the energy range 3–8 eV by implementing the first-principles molecular dynamics method. Although this work computed the temperature effect on optical properties, it only considered the optical properties of SiC in ultraviolet region in which the photon was coupled with electron. However, what we are interested is the optical properties in the infrared region in which the photon is coupled with phonon.

In this work, we carry out the ellipsometric measurements to measure the infrared optical properties of 4H- and 6H-SiC at temperature up to 593 K. We also adopt first-principles calculations to parameterize the Lorentz model and predict the infrared reflectance of 3C-, 4H- and 6H-SiC. In first-principles calculations, we implement density functional perturbation theory (DFPT) calculations to obtain the high frequency dielectric constant and the infrared phonon mode frequency at ground state. The temperature-dependent phonon damping is calculated based on anharmonic lattice dynamics method, in which the harmonic and anharmonic interatomic force constants are calculated from first-principles calculations. The temperature range is extended to 1000 K in the first-principles calculations to investigate the temperature effect. The calculated semi-infinite normal reflectance of SiC is compared with the experimental results. Besides, the effect of temperature and crystal anisotropy on infrared reflectance is also discussed.

2. Experimental measurement and numerical simulation

2.1. Experimental measurement

2.1.1. Ellipsometry equations

The ellipsometric measurements are described through the ellipsometry parameters Ψ and Δ which are defined by Ref. [22].

$$\rho \equiv \frac{r_p}{r_s} = \tan \Psi \exp(i\Delta), \tag{1}$$

where ρ is the complex ratio of samples with plane parallel boundary for the *p*- and *s*-polarized reflectance coefficients r_p and r_s. The right-handed {*x*,*y*,*z*} laboratory coordinate system is determined by the sample surface (*x*-*y* plane) and its normal (*z*-axis). The origin of {*x*,*y*,*z*} is set at the sample surface, and the *x* axis is parallel to the plane of incidence, which is defined by the incident and reflected light beams [23].

For isotropic bulk materials, the dielectric function values can be determined by the isotropic two-phase (ambient-substrate) model [22,24].

$$\varepsilon \equiv \{1 + [(1-\rho(\omega))/(1+\rho(\omega))]\tan^2\theta_a\}\sin^2\theta_a, \tag{2}$$

where θ_a is the angle of incidence. For anisotropic bulk materials, the ellisometric measurements depend on the principal axis dielectric function values ε_x, ε_y, ε_z, the orientation of the crystal principal axes with respect to the plane of incidence, and the polarization state of the incident light beam. Based on the generalized ellipsometry approach [23,25], the *p*- and *s*-polarized reflectance coefficients r_p and r_s used in Eq. (1) are

$$r_p = \frac{N_{xa} - N_{az}}{N_{az} + N_{xa}}, \tag{3}$$

$$r_s = \frac{N_{aa} - N_{yy}}{N_{aa} + N_{yy}}, \tag{4}$$

with

$$N_{ij} = \sqrt{\varepsilon_i}\sqrt{1 - \frac{1}{\varepsilon_j}\sin^2\theta_a}. \tag{5}$$

For anisotropic sample measurements, direct inversions of the ellipsometric parameters Ψ and Δ into ε_x, ε_y, ε_z, as in Eq. (2) for the isotropic case, do not exist, and numerical regression procedures are needed for data analysis to extract the dielectric constant from Eqs. (3)–(5). Furthermore, in order to obtain sufficient information about ε_x, ε_y and ε_z, the measurements at variable angles of incidence are necessary.

2.1.2. Preparation and measurement

In the experimental measurements, commercially available 4H- and 6H-SiC wafers with diameter of 100 mm and thickness of 350 μm were purchased from TankeBlue CO., LTD. The wafer orientation of these samples was along the *c*-axis, which meant that the *c*-axis was perpendicular to the sample surface. The dielectric constant of 4H- and 6H-SiC were obtained based on the ellipsometric parameters Ψ and Δ measured by spectroscopic ellipsometry. The measurement data were obtained at 70° and 75° angle of incidence for the *c*-plane sample surface (*c*-axis was perpendicular to the sample surface). The high temperature (593 K) in the measurement was obtained by using temperature controller purchased from Instec, Inc.

2.2. Numerical simulation

2.2.1. Infrared dielectric model

For uniaxial materials, the infrared absorption is associated with the crystal anisotropy, such as 4H- and 6H-SiC with hexagonal lattice structure. Fig. 1 shows the lattice structure of the unit cell of 3C-, 4H- and 6H-SiC. The stacking order of the Si-C bilayers is A-B-C, A-B-C-B and A-B-C-A-C-B for 3C-, 4H- and 6H-SiC, which leads to a hexagonal structure along the stacking direction (*c*-axis) for 4H- (four silicon and carbon atoms per unit cell) and 6H-SiC (six silicon and carbon atoms per unit cell), respectively [8]. It should be noted that the 3C-SiC is not uniaxial crystal, since all Si-C bilayer shifts occur in the same direction and reach an identical position along the hexagonal axis after three stacking steps, which results in a structure with cubic symmetry. The crystal anisotropy of 4H- and 6H-SiC is reflected from the hexagonal structure [26,27], which means that the properties along *a*-axis or *b*-axis are different from that along *c*-axis. These uniaxial materials show some polarization-dependent infrared absorption due to the anisotropy.

Generally, there exist two different solutions of the wave equations in uniaxial media, which describe the ordinary and the extraordinary rays [28]. The ordinary ray is the light with electric vector perpendicular to *c*-axis, while the extraordinary ray is the light with electric vector parallel to *c*-axis. The frequency-dependent dielectric function of uniaxial material in infrared region has been discussed theoretically in Refs. [26,28]. As described there, the explicit forms of the dielectric function are given by

$$\varepsilon_\perp(\omega) = \varepsilon_\perp^\infty + \sum_{j=1}^{v} \frac{S_{\perp,j}\omega_{\perp,j}^2}{\omega_{\perp,j}^2 - \omega^2 - i\gamma_{\perp,j}\omega}, \tag{6}$$

$$\varepsilon_\parallel(\omega) = \varepsilon_\parallel^\infty + \sum_{k=1}^{w} \frac{S_{\parallel,k}\omega_{\parallel,k}^2}{\omega_{\parallel,k}^2 - \omega^2 - i\gamma_{\parallel,k}\omega}, \tag{7}$$

where *v* and *w* are the number of resonant modes which are perpendicular and parallel to *c*-axis, respectively.

These equations are parameterized with the resonant frequencies, damping factor and oscillator strength. It should be noted that the

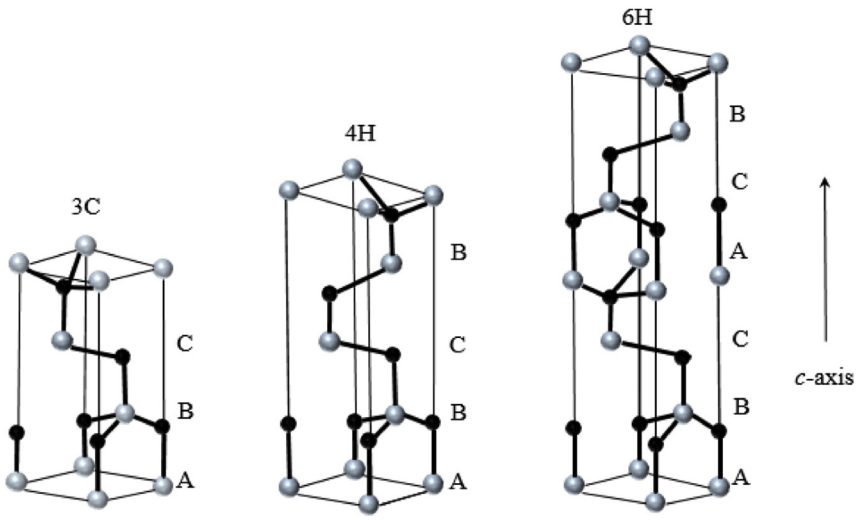

Fig. 1. Lattice structure of the unit cell of 3C-, 4H- and 6H-SiC.

resonant modes in these equations are associated with the phonon modes which have very small momentum (approach to zone-center Γ, $q \rightarrow 0$) due to the negligible momentum of photons compared to phonons. Many efforts have been devoted to establishing a relationship between the parameters and the phonon properties. Based on Born and Huang's phenomenological theory [29], Bao *et al.* [30] derived the frequency-dependent dielectric function of a diatomic ionic material with cubic symmetry. For the hexagonal structure SiC, there are large number of infrared active phonons (six and ten IR active branches [31] for 4H- and 6H-SiC, respectively). In these infrared active modes, there are strong infrared modes with large net polarization resulting from all the silicon atoms displaced opposite to carbon atoms, while the others are weak modes which can be neglected [26,27]. Therefore, it is sufficient to regard only the strong infrared modes in the dielectric function of uniaxial SiC [11], Using the generalized Lyddane-Sachs-Teller (LST) [32] relationship and neglecting the mode coupling, the dielectric function can be reduced to be [11].

$$\frac{\varepsilon_j(\omega)}{\varepsilon_j(\infty)} = 1 + \frac{\omega_{j,\mathrm{LO}}^2 - \omega_{j,\mathrm{TO}}^2}{\omega_{j,\mathrm{TO}}^2 - \omega^2 - i\gamma_j\omega}, \quad j = \parallel, \perp \tag{8}$$

where $\omega_{\perp,\mathrm{LO}}(\omega_{\perp,\mathrm{TO}})$ and $\omega_{\parallel,\mathrm{LO}}(\omega_{\parallel,\mathrm{TO}})$ are the zone-center (approaching to Γ point) frequencies of the longitudinal and transverse infrared active phonon mode that are perpendicular and parallel to *c*-axis, respectively.

Therefore, the parameterized equation can be determined if the high frequency dielectric constant $\varepsilon(\infty)$, infrared active TO phonon frequency ω_{TO} and corresponding LO phonon frequency ω_{LO}, and the TO phonon damping γ are known. Generally, these parameters, especially the phonon damping factor, are not easy to predict from theoretical theory, which are usually determined by fitting to experimental data.

The lifetime τ_λ with single mode relaxation time approximation of phonon mode (λ) can be calculated through the anharmonic lattice method, in which the harmonic and anharmonic interatomic force constants are determined from first-principles calculations [33]. Generally, the relaxation time is inversely proportional to the phonon damping. Therefore, the TO phonon damping γ_{TO} can be obtained [34].

$$\gamma_{\mathrm{TO}} = \frac{1}{\tau_{\mathrm{TO}}}. \tag{9}$$

In this work, the high frequency dielectric constant is determined by the first-principles calculation based on the density functional perturbation theory. The frequency of infrared phonon mode is obtained through the atomic vibration analysis based on first-principles calculations. The phonon damping factor associated with the phonon lifetime is obtained with the calculated harmonic and anharmonic interatomic force constants from first-principles calculations.

2.2.2. Simulation details

In our work, first-principles calculations were carried out using the VASP [35] package. The projector augmented-wave (PAW) [36] method and the Perdew-Burke-Ernzerhof (PBE) [37] exchange and correlation were used in our calculations. The plane-wave energy cutoff was chosen as 360eV. The electronic stopping criterion was 10^{-8} eV. The initial cubic (3C-SiC) and hexagonal (4H- and 6H-SiC) unit cell was generated and optimized with $9 \times 9 \times 9$, $9 \times 9 \times 7$ and $11 \times 11 \times 9$ Monkhorst-Pack automatically generated *k*-mesh until the modulus of the force acting on each atom was less than 1.1×10^{-5} eV/Å, 2.3×10^{-4} eV/Å and 9.2×10^{-4} eV/Å and the external pressure was 0.02 kB, 0.07 kB and −0.04 kB after optimization for 3C-, 4H- and 6H-SiC, respectively. After the geometry optimization, the calculated lattice constant *a* for the cubic 3C-SiC was 4.3591 Å (4.3596 Å from the experiment [38]), the lattice parameters *a* and *c* for the hexagonal 4H-SiC was 3.0939 Å and 10.1287 Å (3.0798 Å and 10.0819 Å from the experiment [39]), and the lattice parameters *a* and *c* for the hexagonal 6H-SiC was 3.0947 Å and 15.1854 Å (3.0805 Å and 15.1151 Å from the experiment [39]). The optimized unit cell was used to compute the harmonic interatomic force constants (IFCs) required for the phonon dispersion calculation. The Phonopy [40] package was used to compute and diagonalize the dynamical matrix and obtain the phonon dispersion curve. The $4 \times 4 \times 4$, $4 \times 4 \times 2$ and $4 \times 4 \times 2$ supercell was created to compute the anharmonic IFCs required for the phonon lifetime calculation. The anharmonic IFCs was computed by the code called THIRDORDER.PY from ShengBTE [33] package. It should be noted that the fourth-nearest neighbors was considered in this calculation. Finally, the ShengBTE package was used to compute the phonon lifetime with the harmonic and anharmonic IFCs.

3. Results and discussion

3.1. Infrared phonon modes of SiC

A detail study of the phonon dispersion relation of 3C-, 4H- and 6H-SiC have been carried out by using the harmonic force constants based on first-principles calculation in VASP [35]. In addition, due to the polarization induced when the atom displaced in ionic solids (such as SiC), the Born effective charges (Z^B) [41] are defined to analyze the LO-TO optical phonon splitting at zone center of Brillion zone in polar crystals. The macroscopic electrostatic interaction of Z^B in turn alters the frequencies of certain longitudinal phonon modes and causes the LO-TO splitting at Γ point. The Born effective charges and the high dielectric constants are obtained by running the perturbative calculations [33], which are in

Table 1
Born effective charge and high frequency dielectric constants of 3C-, 4H- and 6H-SiC in the plane of perpendicular and parallel to *c*-axis, respectively.

Polytype		$(Z^B)_{\|\|}$	$(Z^B)_{\perp}$	$(\varepsilon_\infty)_{\|\|}$	$(\varepsilon_\infty)_{\perp}$
3C	Calculated	2.69	2.69	6.95	6.95
	Ab initio [42]	2.72	2.72	7.02	7.02
4H	Calculated	2.85	2.66	7.27	6.97
	Ab initio [42]	2.78	2.69	7.17	6.95
6H	Calculated	2.74	2.67	7.26	7.02
	Ab initio [42]	2.75	2.68	7.24	7.02

good agreement with others' Ab initio calculations [42] as shown in Table 1. Using the calculated Z^B, the full phonon dispersion curve can be obtained, as shown in Fig. 2.

From Fig. 2, we can see that there exists a discontinuous at Γ point between several optical branches along different propagation directions Γ→A or Γ→K of the phonons in 4H-and 6H-SiC. This is a characteristic feature for hexagonal polytypes, in general for uniaxial crystals [43,44]. Generally, the irreducible representation associated with the symmetry operation in point group is used to identify the phonon modes at Γ point [45]. The phonon modes for hexagonal polytypes 4H- and 6H-SiC with the space group C_{6v} are represented by A_1, E_1, E_2 and B_1. The A_1 and E_1 are both Raman active and infrared active modes, whereas E_2 is only Raman active mode and B_1 is the inactive mode. The long-wavelength optical phonon modes are classified into strong modes and weak modes determined by the atomic displacements. For strong modes, a strong electric field is created due to the opposite vibration of Si and C atom, which results in the frequency of LO is higher than that of TO mode. For weak modes, only very weak electric field is induced by the small intracell motions [27].

These modes can be identified through the atomic displacement along different direction respect to Γ point. The atomic displacement of each mode can be visualized through V_Sim [46] which is interfaced to the Phonopy [40] package. As an example, the atomic displacement of atoms of 4H-SiC that corresponds to strong and weak infrared mode (A_1 and E_1) are visualized as shown in Fig. 3. From Fig. 3(a), it can be seen that all Si atoms are displaced opposite to all the C atoms for the strong infrared phonon mode in both A_1 and E_1 mode. Fig. 3(b) shows the atomic displacement for the weak infrared phonon modes, we can see that the Si and C atoms are intracell moved.

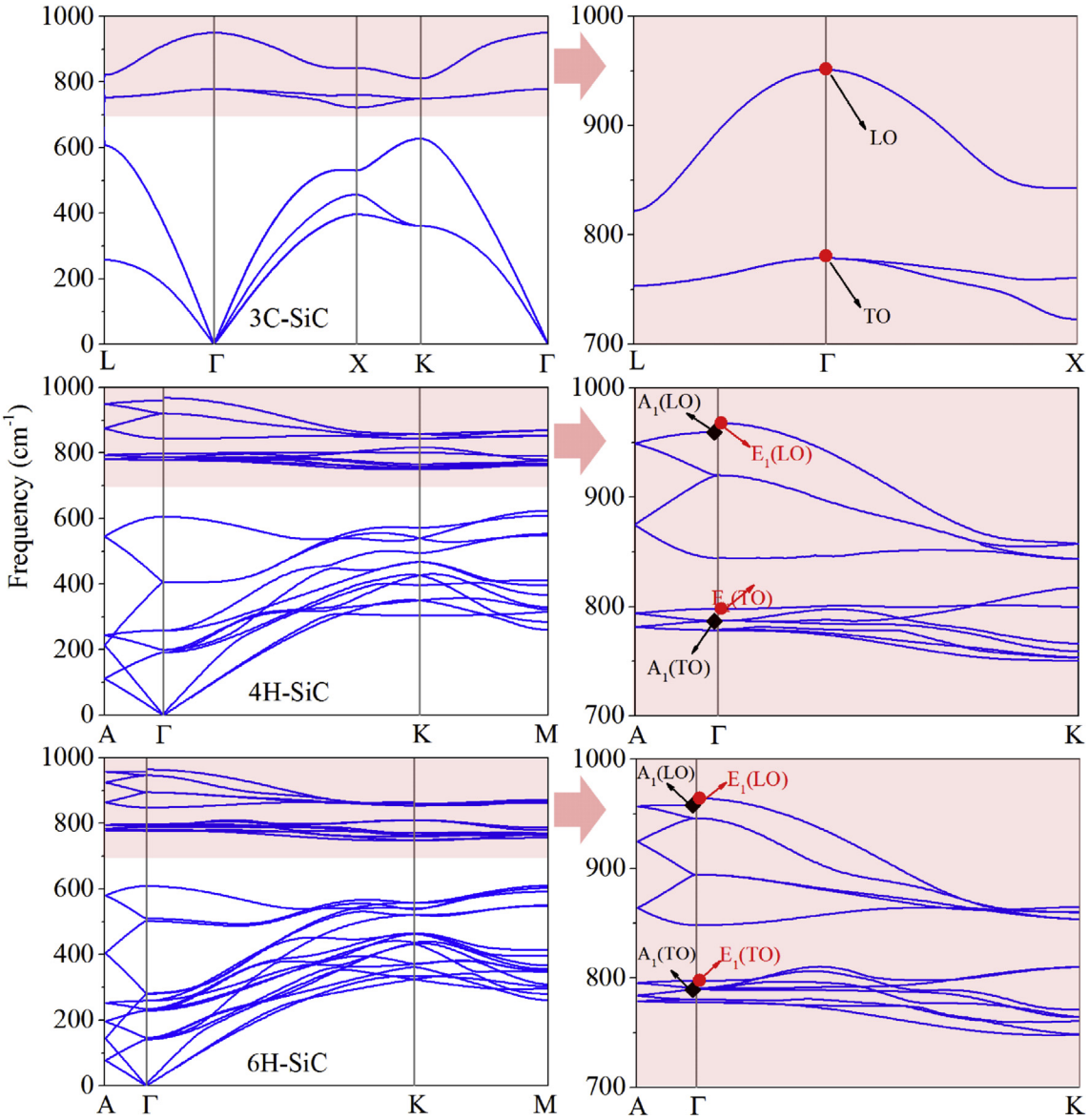

Fig. 2. Phonon dispersion curves of the 3C-, 4H- and 6H-SiC polytypes along high-symmetry lines in the Brillion zone, and the strong infrared phonon mode at zone center.

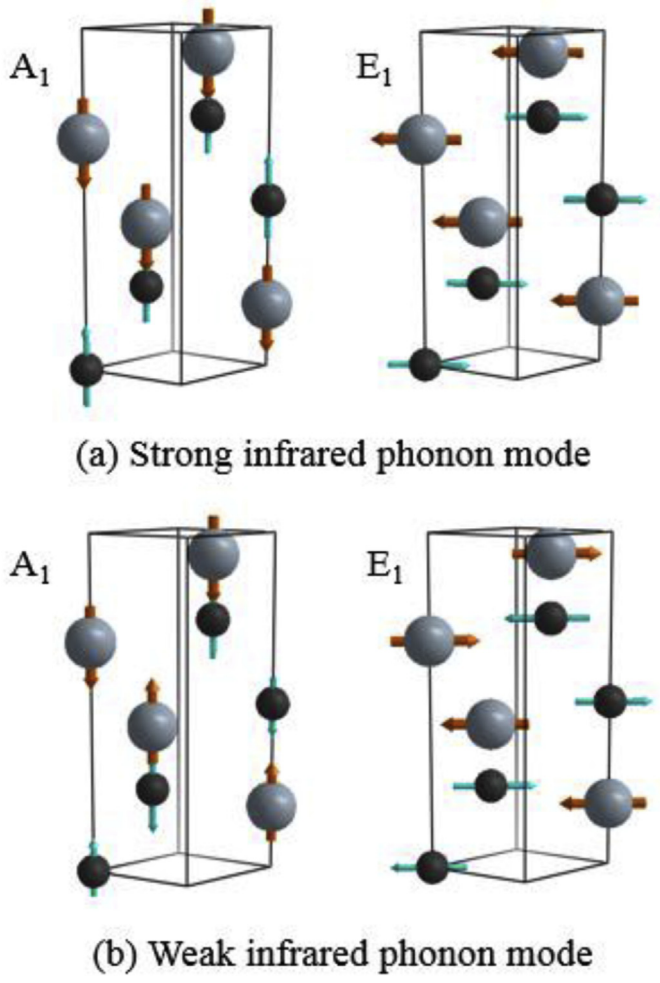

Fig. 3. Atomic displacement of atoms (Si: Gray, C: Black) of 4H-SiC corresponding to the infrared phonon mode. (a) for strong infrared phonon mode of A_1 and E_1, (b) for weak infrared phonon mode of A_1 and E_1.

In addition, the frequency at Γ point ($\mathbf{q} = \mathbf{0}$) of A_1 (or E_1) branches depends on the direction in reciprocal space in which the branch is followed to the zone center [12,45]. For A_1 mode, along Γ→A directions (*z*-axis), the frequency is that of the longitudinal component; along Γ→K directions (in *xy* plane), the frequency is that of the transverse component [45]. Based on this theory and the visualization of the atomic displacement, the frequency of strong infrared phonon modes corresponding to the transverse and longitudinal branches are determined. Along Γ→A direction, the frequency of LO ($\omega_{\parallel LO}$) and TO ($\omega_{\perp TO}$) mode can be obtained through the identified strong A_1 and E_1 mode, respectively. Similarly, the frequency of TO ($\omega_{\parallel TO}$) and LO ($\omega_{\perp LO}$) mode can be obtained through identified strong A_1 and E_1 mode along Γ→K direction, respectively. Moreover, the strong infrared phonon modes were marked in the phonon dispersion curves at zone center, as shown in Fig. 2. The frequency quantities of $\omega_{\perp TO}(\omega_{\perp LO})$ and $\omega_{\parallel TO}(\omega_{\parallel LO})$ determined by this method were in good agreement with the experimental values, as shown in Table 2.

3.2. Temperature-dependent damping factor of SiC

In the present work, the phonon lifetime was obtained through the harmonic and anharmonic IFCs which were calculated from first-principles calculations. Using this method, the temperature-dependent TO phonon mode damping can be calculated. As shown in Fig. 4, we can see that the phonon damping increases with temperature increasing. This is mainly attributed to the increase of phonon-phonon scattering with higher temperature. This work indicates that this method can directly obtain the phonon damping to parameterize the dielectric function and predict the infrared optical properties.

3.3. Dielectric function spectrum

With these obtained values (ε_∞, ω_{LO}, ω_{TO} and γ), the dielectric function in Eq. (8) is fully parameterized. Therefore, the dielectric function spectrum can be obtained, as shown in Fig. 5. From Fig. 5, we can see that the resonance occurs at 12.7 μm for 3C-SiC, 12.7 μm (⊥ *c*-axis) and 12.9 μm (|| *c*-axis) for 4H-SiC, and 12.7 μm (⊥ *c*-axis) and 12.8 μm (|| *c*-axis) for 6H-SiC, which are in well agreement with experimental values [9,10]. After obtaining the dielectric function, the semi-infinite normal reflectance (*R*) can be calculated. The calculated reflectance was compared with the experimental results, as shown in Fig. 6. It should be noted that the experimental values of 4H- and 6H-SiC are obtained using the isotropic model as in Eq. (2), which is due to the failure of regression fitting of Eqs. (3)–(5) for our measurement data though having tried our best to fit it. Some reasons for these unsuccessful regression fitting attribute to the samples (not pure, defects, etc.) and the weak anisotropy in 4H- and 6H-SiC. Moreover, the experimental values of 3C-SiC are extracted from Ref. [12]. From the comparison, it can be seen that the reflection features in our predictions are nearly the same with the experimental measurements, which increases the confidence in our calculations. The two results match well at short and long wavelengths but differ a little (a small drop of the experimental results) within the region of 10–13 μm. The similar behavior was also observed in others' experiment work [9–11], in which attributed it to the surface treatment of the experimental samples.

3.4. Temperature effect on the semi-infinite normal reflectance

Moreover, the SiC has been reported to be used in astronomy, in which the optical constants are important parameters for its application [12,47]. In the astrophysical environments, the temperature-dependent optical constants are significant in these applications. Therefore, the temperature-dependent semi-infinite normal reflectance was studied in this work. As it can be seen that all the parameters in Eq. (8) are temperature-dependent, but the temperature effect is more significant on the phonon damping and it can be neglected on phonon frequency in our interest temperature range. Based on this, the temperature-dependent phonon damping was calculated from first-principles calculations as shown in Fig. 4. Using the parameterized dielectric function, the temperature-dependent semi-infinite normal reflectance was calculated as shown in Fig. 6. It should be noted that we just experimentally

Table 2
Frequencies of the strong infrared phonon modes of 3C-, 4H- and 6H-SiC polytypes. E_{1T} ($\omega_{\perp TO}$) and E_{1L} ($\omega_{\perp LO}$) denotes the frequencies of TO and LO modes in the plane of perpendicular to *c*-axis, respectively, whereas A_{1T} ($\omega_{\parallel TO}$) and A_{1L} ($\omega_{\parallel LO}$) denotes those parallel to *c*-axis.

Polytype	Mode	Calculated (cm^{-1})	Experiment [11] (cm^{-1})	Mode	Calculated (cm^{-1})	Experiment [11] (cm^{-1})
3C	TO	785.5	795.9	LO	955.7	972.3
4H	E_{1T}	798.1	796.6	E_{1L}	967.6	968.7
	A_{1T}	782.4	783.6	A_{1L}	959.5	964.2
6H	E_{1T}	797.5	797.0	E_{1L}	964.2	969.9
	A_{1T}	786.9	788.1	A_{1L}	957.8	965.3

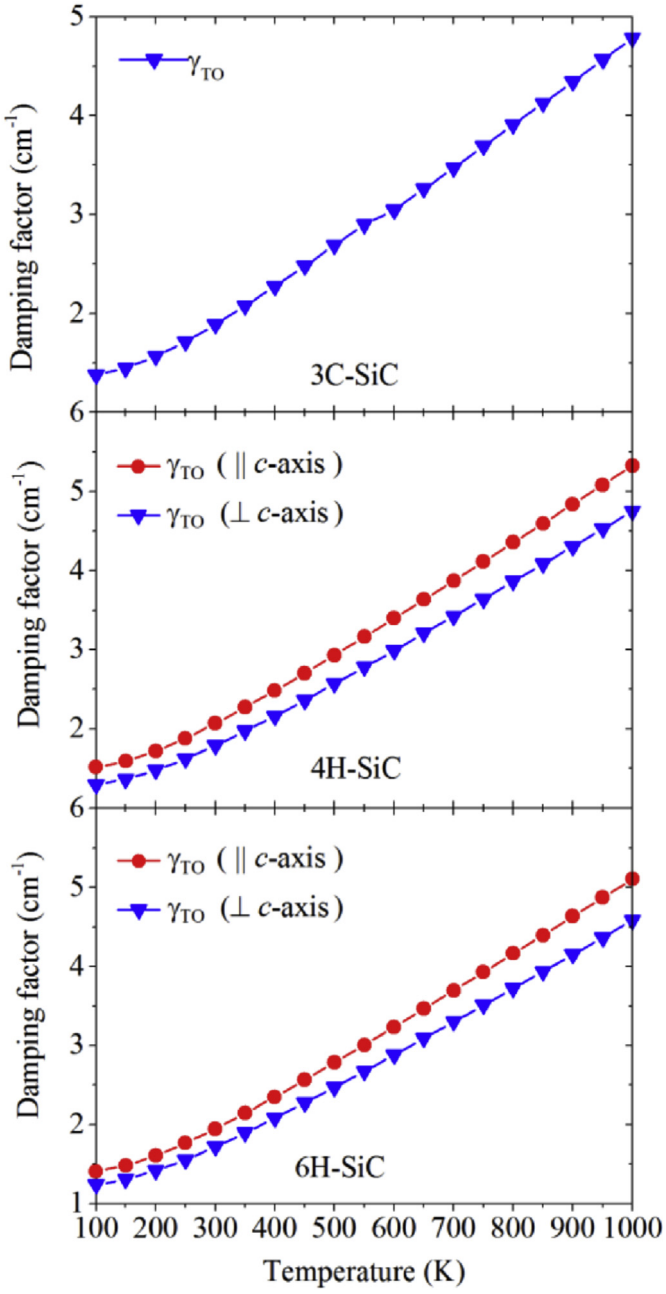

Fig. 4. Temperature dependent of TO phonon damping of 3C-, 4H- and 6H-SiC in the plane of perpendicular and parallel to *c*-axis, respectively.

measure the reflectivity of 4H-SiC and 6H-SiC at 293 K and 593 K, whereas the experimental data for 3C-SiC can be referred to Ref. [12] and just at 293 K. Actually, it is not easy to experimentally measure the optical properties at high temperatures but the elevated temperature effect can be directly predicted in our numerical simulations. From this Fig. 6, it shows that a small reduced peak of the reflectivity in range of 10–13 μm is induced with temperature increasing, but this effect is not significant even though the temperature approaches to 1000 K.

3.5. Anisotropic effect on the semi-infinite normal reflectance

In addition, we also compare the reflectivity among these SiC polytypes, which are shown in Fig. 7. We can see that 3C-SiC and hexagonal-SiC (4H-, 6H-) have almost identical reflection spectrum in the plane of perpendicular to *c*-axis, whereas a little shift exists in the reflection band

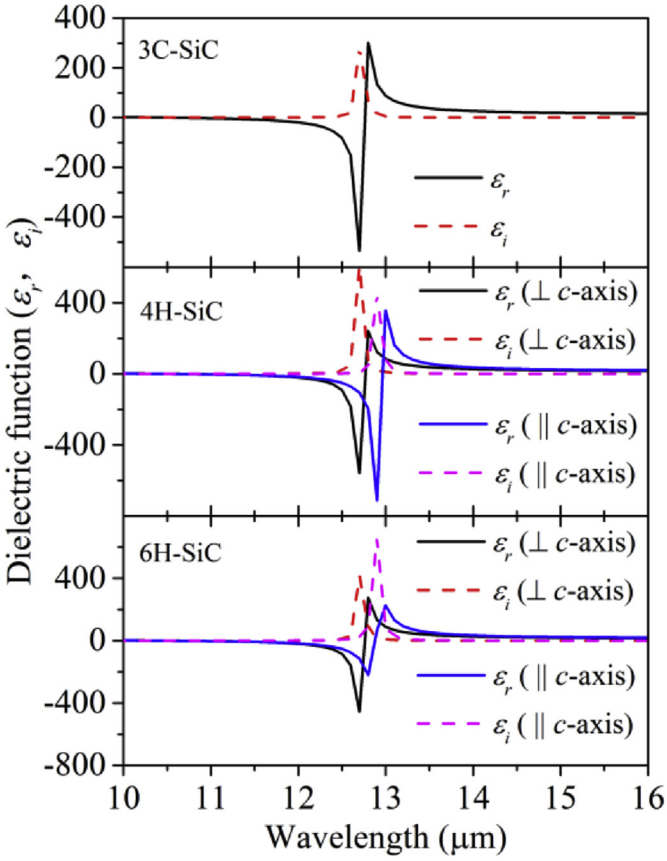

Fig. 5. The calculated dielectric function of 3C-, 4H- and 6H-SiC in the plane of perpendicular and parallel to *c*-axis, respectively.

for plane parallel to *c*-axis. The small shifts existed in the plane of parallel to *c*-axis are attributed to the fact that the main difference among SiC polytypes caused by Si-C bilayer stacking along *c*-axis.

4. Summary

By performing ellipsometric measurements and first-principles calculations, the temperature-dependent optical properties of cubic (3C) and hexagonal (4H and 6H) silicon carbide were investigated in infrared range of 2–16 μm. The experimental values were obtained at 293 K and 593 K. Based on first-principles calculations, the Lorentz model was parameterized without any experimental fitting data and the temperature effect was computed. The frequency of infrared phonon mode was obtained through the atomic vibration analysis based on first-principles calculations. The temperature-dependent damping parameter in the Lorentz model was calculated based on anharmonic lattice dynamics method, in which the harmonic and anharmonic interatomic force constants were calculated from first-principles calculations. We find that the infrared reflection band happens in 10–13 μm wavelength region and the resonance occurs at 12.7 μm for 3C-SiC, 12.7 μm (⊥ *c*-axis) and 12.9 μm (|| *c*-axis) for 4H-SiC, and 12.7 μm (⊥ *c*-axis) and 12.8 μm (|| *c*-axis) for 6H-SiC. Our calculation results are in good agreement with the experimental results at short and long wavelengths but differ a little (a small drop of the experimental results) in the range of 10–13 μm. It is also find that the cubic-SiC and hexagonal-SiC have almost identical reflection spectrum in the plane of perpendicular to *c*-axis, whereas a little shift exists in the reflection spectrum for the plane of parallel to *c*-axis but this effect is not significant. In addition, we find that a small reduction of the reflectivity peak happens in range of 10–13 μm with temperature increasing, but this effect is not significant. Particularly, the temperature range in experimental measurements is limited but our first-principles

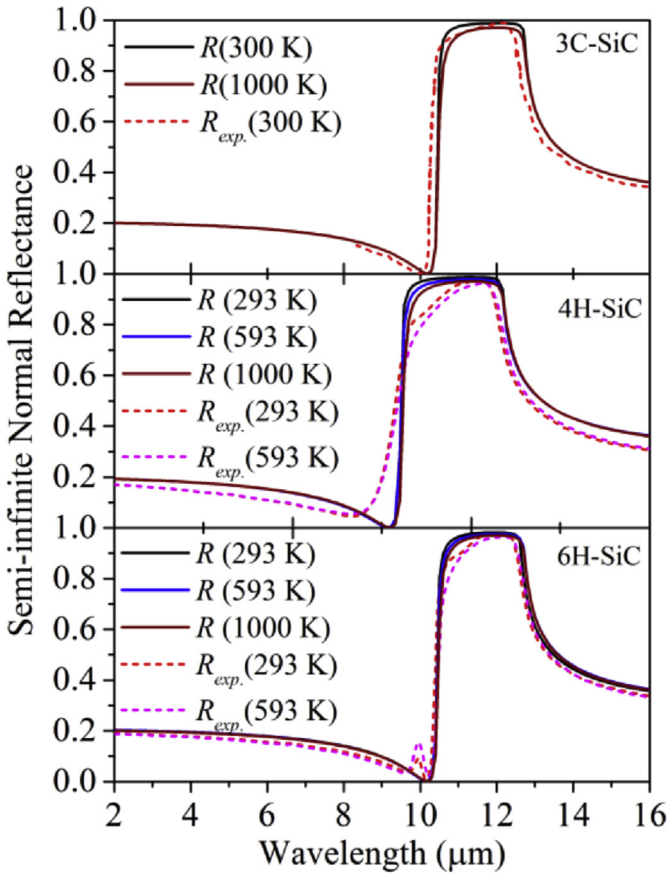

Fig. 6. Semi-infinite normal reflectance of calculated values (solid line) and experimental results (dash line, denoted by '*exp.*').

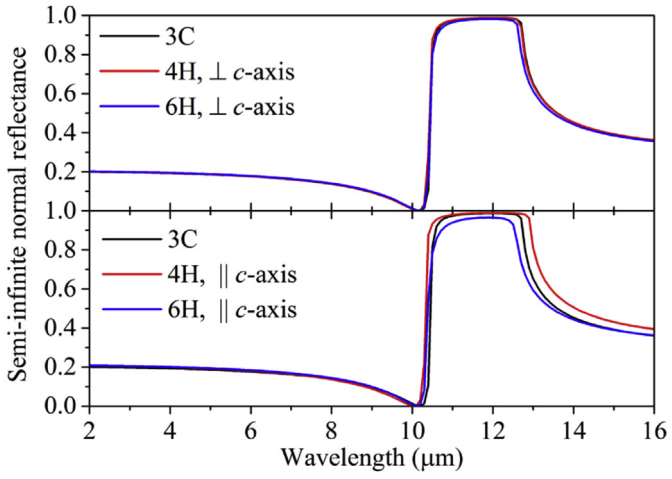

Fig. 7. The calculated semi-infinite normal reflectance at 300 K of 3C-, 4H- and 6H-SiC in the plane of perpendicular and parallel to *c*-axis, respectively.

calculations can predict the infrared optical properties at elevated temperature.

Acknowledgement

This work was supported by the National Natural Science Foundation of China (Grant No. 51676121 and 51336002). Simulations were performed at Center for High Performance Computing (π) of Shanghai Jiao Tong University.

References

[1] J. Fan, P.K. Chu, General properties of bulk SiC, in: Silicon Carbide Nanostructures, Springer, 2014, pp. 7–114.
[2] Z.C. Feng, in: SiC Power Materials: Devices and Applications, vol. 73, Springer Science & Business Media, 2013.
[3] A.R. Powell, L.B. Rowland, SiC materials-progress, status, and potential roadblocks, Proc. IEEE 90 (6) (2002) 942–955.
[4] M. Willander, M. Friesel, Q. Wahab, B. Straumal, Silicon carbide and diamond for high temperature device applications, J. Mater. Sci. Mater. Electron. 17 (1) (2006) 1.
[5] J.B. Casady, R.W. Johnson, Status of silicon carbide (SiC) as a wide-bandgap semiconductor for high-temperature applications: a review, Solid State Electron. 39 (10) (1996) 1409–1422.
[6] S. Agathopoulos, Influence of synthesis process on the dielectric properties of B-doped SiC powders, Ceram. Int. 38 (4) (2012) 3309–3315.
[7] J. Yuan, W.-L. Song, X.-Y. Fang, X.-L. Shi, Z.-L. Hou, M.-S. Cao, Tetra-needle zinc oxide/silica composites: high-temperature dielectric properties at X-band, Solid State Commun. 154 (2013) 64–68.
[8] F. Bechstedt, et al., Polytypism and properties of silicon carbide, Phys. Status Solidi B 202 (1) (1997) 35–62.
[9] W.G. Spitzer, D.A. Kleinman, C.J. Frosch, Infrared properties of cubic silicon carbide films, Phys. Rev. 113 (1) (1959) 133.
[10] W.G. Spitzer, D. Kleinman, D. Walsh, Infrared properties of hexagonal silicon carbide, Phys. Rev. 113 (1) (1959) 127.
[11] H. Mutschke, A.C. Andersen, D. Clément, T. Henning, G. Peiter, Infrared Properties of SiC Particles, 1999. ArXiv Prepr. Astro-Ph9903031.
[12] K.M. Pitman, A.M. Hofmeister, A.B. Corman, A.K. Speck, Optical properties of silicon carbide for astrophysical applications-I. New laboratory infrared reflectance spectra and optical constants, Astron. Astrophys. 483 (2) (2008) 661–672.
[13] O.P.A. Lindquist, M. Schubert, H. Arwin, K. Järrendahl, Infrared to vacuum ultraviolet optical properties of 3C, 4H and 6H silicon carbide measured by spectroscopic ellipsometry, Thin Solid Films 455 (2004) 235–238.
[14] H.-J. Yang, et al., Silicon carbide powders: temperature-dependent dielectric properties and enhanced microwave absorption at gigahertz range, Solid State Commun. 163 (2013) 1–6.
[15] J. Petalas, S. Logothetidis, M. Gioti, C. Janowitz, Optical properties and temperature dependence of the interband transitions of 3 C- and 6 H-SiC in the energy region 5 to 10 eV, Phys. Status Solidi B 209 (2) (1998) 499–521.
[16] C. Cobet, K. Wilmers, T. Wethkamp, N.V. Edwards, N. Esser, W. Richter, Optical properties of SiC investigated by spectroscopic ellipsometry from 3.5 to 10 eV, Thin Solid Films 364 (1) (2000) 111–113.
[17] H. Fujiwara, Spectroscopic Ellipsometry: Principles and Applications, John Wiley & Sons, 2007.
[18] C. Xie, P. Xu, F. Xu, H. Pan, Y. Li, First-principles studies of the electronic and optical properties of 6H–SiC, Phys. B Condens. Matter 336 (3) (2003) 284–289.
[19] W.R. Lambrecht, S. Limpijumnong, S.N. Rashkeev, B. Segall, Electronic band structure of SiC polytypes: a discussion of theory and experiment, Phys. Status Solidi B 202 (1) (1997) 5–33.
[20] G. Domingues, A.M. Mothe, S. Guevelou, B. Rousseau, Study by molecular dynamics of the influence of temperature and pressure on the optical properties of undoped 3C-SiC structures, J. Quant. Spectrosc. Radiat. Transf 205 (2018) 220–229.
[21] J.Y. Yang, L.H. Liu, J.Y. Tan, First-principles molecular dynamics study on temperature-dependent dielectric function of bulk 3C and 6H SiC in the energy range 3–8eV, Phys. B Condens. Matter 436 (2014) 182–187.
[22] R.M. Azzam, N.M. Bashara, Ellipsometry and Polarized Light. North-Holland. Sole Distributors for the USA and Canada, Elsevier Science Publishing Co., Inc., 1987.
[23] M. Schubert, Generalized ellipsometry and complex optical systems, Thin Solid Films 313 (1998) 323–332.
[24] M. Schubert, T.E. Tiwald, C.M. Herzinger, Infrared dielectric anisotropy and phonon modes of sapphire, Phys. Rev. B 61 (12) (2000) 8187.
[25] M. Schubert, Polarization-dependent optical parameters of arbitrarily anisotropic homogeneous layered systems, Phys. Rev. B 53 (8) (1996) 4265.
[26] F. Engelbrecht, R. Helbig, Effect of crystal anisotropy on the infrared reflectivity of 6H-SiC, Phys. Rev. B 48 (21) (1993), 15698.
[27] L. Patrick, Infrared absorption in SiC polytypes, Phys. Rev. 167 (3) (1968) 809.
[28] R. Loudon, The Raman effect in crystals, Adv. Phys. 13 (52) (1964) 423–482.
[29] M. Born, K. Huang, Dynamical Theory of Crystal Lattices, Oxford university press, 1998.
[30] H. Bao, B. Qiu, Y. Zhang, X. Ruan, A first-principles molecular dynamics approach for predicting optical phonon lifetimes and far-infrared reflectance of polar materials, J. Quant. Spectrosc. Radiat. Transf. 113 (13) (2012) 1683–1688.
[31] S. Nakashima, H. Harima, Raman investigation of SiC polytypes, Phys. Status Solidi 162 (1) (1997) 39–64.
[32] R.H. Lyddane, R.G. Sachs, E. Teller, On the polar vibrations of alkali halides, Phys. Rev. 59 (8) (1941) 673.
[33] W. Li, J. Carrete, N.A. Katcho, N. Mingo, ShengBTE: a solver of the Boltzmann transport equation for phonons, Comput. Phys. Commun. 185 (6) (2014) 1747–1758.
[34] H. Xie, T. Ouyang, É. Germaneau, G. Qin, M. Hu, H. Bao, Large tunability of lattice thermal conductivity of monolayer silicene via mechanical strain, Phys. Rev. B 93 (7) (2016), 075404.
[35] G. Kresse, J. Furthmüller, Efficiency of ab-initio total energy calculations for metals and semiconductors using a plane-wave basis set, Comput. Mater. Sci. 6 (1) (1996) 15–50.
[36] P.E. Blöchl, Projector augmented-wave method, Phys. Rev. B 50 (24) (1994) 17953.

[37] J.P. Perdew, K. Burke, M. Ernzerhof, Generalized gradient approximation made simple, Phys. Rev. Lett. 77 (18) (1996) 3865.
[38] O. Madelung, Numerical data and functional relationships in science and technology, Landolt Bornstein New Ser. Group III 22 (1982) 117.
[39] M. Stockmeier, R. Müller, S.A. Sakwe, P.J. Wellmann, A. Magerl, On the lattice parameters of silicon carbide, J. Appl. Phys. 105 (3) (2009) 033511.
[40] A. Togo, I. Tanaka, First principles phonon calculations in materials science, Scr. Mater., 108 (2015) 1–5.
[41] K. Karch, P. Pavone, W. Windl, O. Schütt, D. Strauch, Ab initio calculation of structural and lattice-dynamical properties of silicon carbide, Phys. Rev. B 50 (23) (1994) 17054.
[42] G. Wellenhofer, K. Karch, P. Pavone, U. Rössler, D. Strauch, Pressure dependence of static and dynamic ionicity of SiC polytypes, Phys. Rev. B 53 (10) (1996) 6071.
[43] M. Hofmann, A. Zywietz, K. Karch, F. Bechstedt, Lattice dynamics of SiC polytypes within the bond-charge model, Phys. Rev. B 50 (18) (1994) 13401.
[44] V.Y. Davydov, et al., Phonon dispersion and Raman scattering in hexagonal GaN and AlN, Phys. Rev. B 58 (19) (1998) 12899.
[45] H. Ashraf, Investigation of the Symmetries of the Phonons in 4H and 6H-SiC by Infrared Absorption and Raman Spectroscopy, 2005.
[46] V_Sim - home page. [Online]. Available: http://inac.cea.fr/L_Sim/V_Sim/. [Accessed: 12-Sep-2017].
[47] A.M. Hofmeister, K.M. Pitman, A.F. Goncharov, A.K. Speck, Optical constants of silicon carbide for astrophysical applications. II. Extending optical functions from infrared to ultraviolet using single-crystal absorption spectra, Astrophys. J. 696 (2) (2009) 1502.